# A 10-Yr Global Land Surface Reanalysis Interim Dataset (CRA-Interim/Land): Implementation and Preliminary Evaluation

Xiao LIANG[1], Lipeng JIANG[1*], Yang PAN[1], Chunxiang SHI[1], Zhiquan LIU[2], and Zijiang ZHOU[1]

1 *National Meteorological Information Center*, *China Meteorological Administration*, *Beijing* 100081, *China*
2 *National Center for Atmospheric Research*, *Boulder*, *CO* 80301, *USA*

(Received May 30, 2019; in final form December 1, 2019)

ABSTRACT

A land surface reanalysis dataset covering the most recent decades is able to provide temporally consistent initial conditions for weather and climate models, and thus is crucial to verifying/improving numerical weather/climate forecasts/predictions. In this paper, we report the development of a 10-yr China Meteorological Administration (CMA) global Land surface ReAnalysis Interim dataset (CRA-Interim/Land; 2007–2016, 6-h intervals, approximately 34-km horizontal resolution). The dataset was produced and evaluated by using the Global Land Data Assimilation System (GLDAS) and NCEP Climate Forecast System Reanalysis (CFSR) global land surface reanalysis datasets, as well as in situ observations in China. The results show that the global spatial patterns and monthly variations of the CRA-Interim/Land, GLDAS, and CFSR climatology are highly consistent, while the soil moisture and temperature values of the CRA-Interim/Land dataset are in between those of the GLDAS and CFSR datasets. Compared with ground observations in China, CRA-Interim/Land soil moisture is comparable to or better than that of GLDAS and CFSR datasets for the 0–10-cm soil layer and has higher correlations and slightly lower root mean square errors (RMSE) for the 10–40-cm soil layer. However, CRA-Interim/Land shows negative biases in 10–40-cm soil moisture in Northeast China and north of central China. For ground temperature and the soil temperature in different layers, CRA-Interim/Land behaves better than the CFSR, especially in East and central China. CRA-Interim/Land has added value over the land components of CRA-Interim due to the introduction of global precipitation observations and improved soil/vegetation parameters. Therefore, this dataset is potentially a critical supplement to the CRA-Interim. Further evaluation of the CRA-Interim/Land, assimilation of near-surface atmospheric forcing variables, and extension of the current dataset to 40 yr (1979–2018) are in progress.

**Key words:** global land surface reanalysis dataset, CRA-Interim/Land, ground temperature, soil temperature, soil moisture, Global Land Data Assimilation System (GLDAS)

**Citation:** Liang, X., L. P. Jiang, Y. Pan, et al., 2020: A 10-yr global land surface reanalysis interim dataset (CRA-Interim/Land): Implementation and preliminary evaluation. *J. Meteor. Res.*, **34**(1), 101–116, doi: 10.1007/s13351-020-9083-0.

## 1. Introduction

Land surface processes regulate the water and energy fluxes at the land–atmosphere interface; therefore, these processes and their initial conditions in models have an important role in weather and climate forecasts. A land surface reanalysis dataset covering the most recent decades can provide temporally consistent initial land conditions for weather and climate models, and thus is crucial to improvement of numerical weather forecasts and to verification of seasonal climate forecasting systems.

In 2014, the China Meteorological Administration (CMA) started its mission to producing China's first generation of a 40-yr global atmospheric reanalysis product (CRA-40; Liu et al., 2017). So far, a 10-yr CMA global atmospheric ReAnalysis Interim dataset (CRA-Interim) covering the period 2007–2016 has been completed. More recently, the production of a CRA-40 dataset from

Supported by the China Meteorological Administration Special Public Welfare Research Fund (GYHY201506002), National Key Research and Development Program of China (2018YFC1506601), National Natural Science Foundation of China (91437220), and National Innovation Project for Meteorological Science and Technology (CMAGGTD003-5).

*Corresponding author: jianglp@cma.gov.cn.

1979 to near real time has commenced. In addition to atmospheric conditions, reanalysis products also provide estimates of land surface fields, including land surface fluxes and state variables (sensible and latent heat fluxes, ground temperature, soil moisture, snow, etc.). However, such land surface simulations are directly forced by the output of near-surface meteorological fields (precipitation, radiation, air temperature, humidity, etc.) from the atmospheric reanalysis system. Owing to considerable biases in land surface forcings (especially precipitation) from the companion atmospheric model, the land surface variables are unavoidably subject to non-trivial errors and drifts (Maurer et al., 2001; Gottschalck et al., 2005), and therefore fail to meet the requirement of many applications, such as land surface water budget studies and the initialization of numerical weather prediction models. To overcome such problems, many global atmospheric reanalysis projects have generated alternative land reanalysis datasets using offline land-only simulations, such as the land surface dataset of ECMWF Interim reanalysis (ERA-Interim/Land; Balsamo et al., 2015), the ongoing land surface dataset of the fifth generation of ECMWF reanalysis (ERA5/Land; Joaquin et al., 2017), the land surface dataset of the Modern-Era Retrospective analysis for Research and Applications (MERRA-Land; Reichle et al., 2011), and the weakly coupled NCEP Global Land Data Assimilation System for the Climate Forecast System Reanalysis (CFSR/GLDAS; Meng et al., 2012; Xia et al., 2019). Similarly, in association with the CRA-Interim reanalysis, we have produced the CMA global Land surface ReAnalysis Interim (CRA-Interim/Land) dataset, a 10-yr (2007–2016) global land surface reanalysis dataset. With higher accuracy of land surface variables due to the introduction of improved global soil/vegetation parameters and observed global precipitation, the offline CRA-Interim/Land dataset is potentially a critical supplement to the land surface component of the CRA-Interim.

To produce the CRA-Interim/Land dataset, near-surface meteorological fields from the CRA-Interim (Liu et al., 2017) are used to force the Noah land surface model. Among all the land forcing variables, the accuracy of precipitation is the most important for reasonable land surface simulation (Decharme and Douville, 2006; Guo et al., 2006; Materia et al., 2010). To alleviate substantial biases in the reanalysis precipitation to prevent the estimated land surface variables from drifting too far, we use observation-based global precipitation analysis as an alternative forcing to enhance land simulations. The global soil and vegetation datasets are also updated for the Noah model.

This paper documents the implementation and evaluation of the CRA-Interim/Land product (6-h intervals, approximately 34-km Gaussian grid). Section 2 details the methods and datasets used to generate and evaluate the CRA-Interim/Land dataset. Section 3 describes and discusses the main evaluation results for soil moisture, soil temperature, and ground temperature against in situ observations and other similar global land reanalysis products. A brief summary is provided in Section 4.

## 2. Data and model

The CRA-Interim/Land dataset is produced by the offline Noah land surface model (LSM) simulations on a global Gaussian grid (1152 × 576; approximately 34-km horizontal resolution), driven by the 3-hourly near-surface atmospheric forcing fields from the CRA-Interim, which are linearly interpolated to the 30-min time step of the LSM. The output temporal interval is 6 h. The global vegetation information is derived from the modified IGBP (International Geosphere–Biosphere Programme) 20-category classification dataset, including 16 IGBP vegetation classes and 3 classes of Tundra (Friedl et al., 2010). The global soil information is extracted from the STATSGO/FAO 16-category soil texture map, which is a hybrid of the 30-s STATSGO over the continental United States and the 5-min FAO elsewhere (available online at http://websoilsurvey.nrcs.usda.gov). All the input data, including terrain height, land–sea mask, and soil and vegetation parameters, are remapped to the 34-km Gaussian grid before being introduced into the model.

### 2.1 *Forcing and validation data*

Here, we briefly introduce the atmospheric forcing data, particularly the precipitation data used to drive the land surface model, and the validation data used to quantify the accuracy of the CRA-Interim/Land dataset.

#### 2.1.1 *Atmospheric forcing data and blended precipitation*

The forcing variables required to drive the land simulation include the near-surface air temperature, humidity, wind speed, surface pressure, surface downward shortwave and longwave radiation, and precipitation. In many global land reanalysis projects, such as the above-mentioned MERRA-Land, ERA-Interim/Land, and ERA5/Land, most of the forcing variables are directly extracted from the companion atmospheric reanalysis system except that the precipitation is bias corrected. Here, we adopted a similar strategy for the CRA-Interim/Land dataset. The newly developed Chinese first-generation global atmospheric reanalysis, CRA, is based on the NOAA

Global Forecast System (GFS) model and the Gridpoint Statistical Interpolation (GSI) 3DVAR data assimilation system with a T574 spectral resolution (approximately 34-km grid spacing). An interim version of CRA (CRA-Interim; Liu et al., 2017; Zhao et al., 2019) was produced in early 2018 for a 10-yr period (1 January 2007 to 31 December 2016) with 6-h intervals. An abundance of data from conventional observations and multiple satellite instruments, particularly for the East Asian regions, have been assimilated into the CRA-Interim. Most forcing variables of the CRA-Interim/Land dataset are derived from the CRA-Interim reanalysis output, except for the precipitation.

A number of previous studies have shown non-trivial biases in the reanalysis precipitation (e.g., Janowiak et al., 1998; Fekete et al., 2004). To correct such biases in precipitation, we introduced two sets of observation-based global precipitation analyses and blended them with the CRA-Interim reanalysis precipitation, following the method utilized in the CFSR/GLDAS (Meng et al., 2012). One dataset is the CPC Merged Analysis of Precipitation (CMAP; Xie and Arkin, 1997) with a global 5-day mean and a 2.5° horizontal resolution, generated by merging gauge and satellite observations. The other dataset is the CPC unified daily gauge analysis (CPCU; Xie et al., 2007) with a global 0.5° resolution, produced by interpolating quality-controlled gauge observations from more than 30,000 sites using the optimal interpolation method. Considering the global rain gauge and satellite data distribution, the blending weight is designed to be latitude-dependent to integrate the multi-source precipitation datasets into an optimal precipitation forcing dataset. More details about the blending method can be found in Meng et al. (2012).

#### 2.1.2 *Soil moisture and temperature observations in China*

The 10-day manually measured soil moisture observation data from 242 agricultural meteorological observing stations (Fig. 1) during 1981–2010 are strictly quality controlled based on climatic characteristics and soil texture, as well as the theory of extreme values of and the relationship between soil hydrological constants proposed by the National Meteorological Center (NMC) of CMA (Zhang et al., 2017). The dataset contains soil moisture observations and quality control marks at 10 vertical levels/depths: 0–10, 10–20, 20–30, 30–40, 40–50, 50–60, 60–70, 70–80, 80–90, and 90–100 cm.

The ground temperature and soil temperature observations at the national ground meteorological stations (Fig. 2) from 1951 to present (more than 2400 stations since 1979) are archived by the National Meteorological Information Center (NMIC) of CMA after quality control (Ren et al., 2015). The soil temperature observation depths include 0, 5, 10, 15, 20, 40, 80, 160, and 320 cm. These two sets of soil moisture and temperature observations are used to quantify the accuracy of the CRA-Interim/Land products in China.

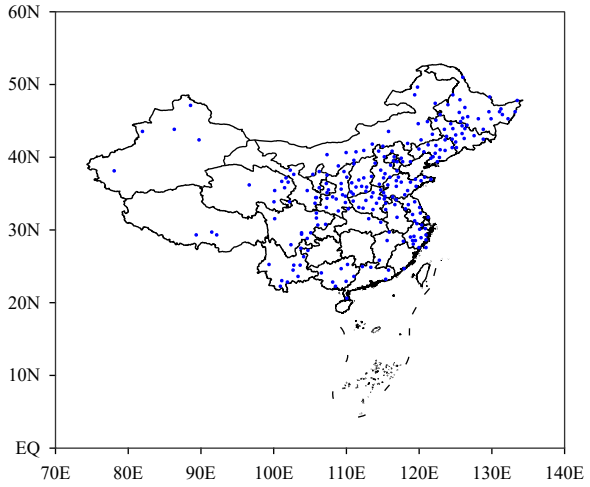


**Fig. 1.** Distribution of 242 agricultural meteorological observation stations in China.

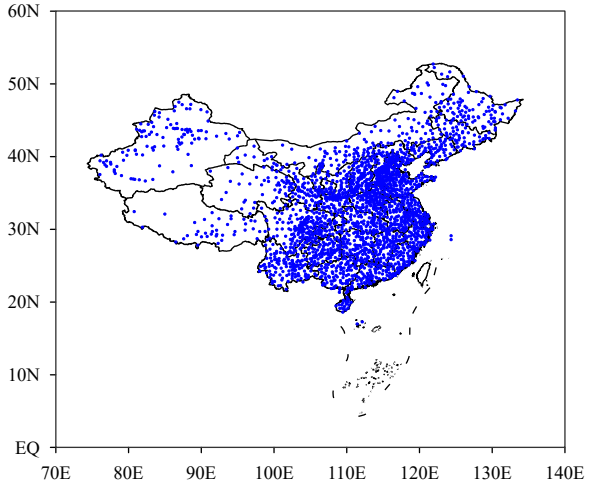


**Fig. 2.** Distribution of more than 2400 national ground meteorological stations in China.

#### 2.1.3 *GLDAS and CFSR global land reanalysis products*

Owing to the lack of large-scale ground observations, it is difficult to quantify the errors of the CRA-Interim/Land globally against observations only. Nevertheless, it is possible to compare CRA-Interim/Land with other similar global land reanalysis products. In this paper, this is done by validating the CRA-Interim/Land against the GLDAS and CFSR global land surface datasets, which use the same Noah-LSM model (but differ-

ent versions) and comparable spatial resolutions.

GLDAS was jointly developed by scientists at NASA and NOAA to generate optimal fields of land surface states by integrating observation-based data products (Rodell et al., 2004). It has been widely evaluated in many studies (e.g., Zaitchik et al., 2010; Jiménez et al., 2011; Decker et al., 2012; Wang and Zeng, 2012; Chen et al., 2013; Xue et al., 2013; Ji et al., 2015) and used in various research fields, such as the estimation of terrestrial water storage changes (e.g., Rodell et al., 2007; Henry et al., 2011; Long et al., 2013; Proulx et al., 2013; Gao et al., 2014), the evaluation of satellite-estimated soil moisture products (e.g., Dorigo et al., 2012; Liu et al., 2012; Kim et al., 2015), and the assessment of land–atmosphere coupling strength (e.g., Zhang et al., 2008; Liu et al., 2014). GLDAS includes outputs from four land surface models: the Community Land Model (CLM), the Noah model, the Mosaic model, and the Variable Infiltration Capacity (VIC) model. In this paper, the GLDAS 0.25° 3-hourly products simulated by the Noah model (GLDAS-2.0) are used for comparison with the CRA-Interim/Land. GLDAS-2.0 is forced by the global meteorological forcing dataset from Princeton University (Sheffield et al., 2006) and aims to create a climatologically consistent dataset from 1948 to 2010. The same soil/vegetation parameters as those used in CRA-Interim/Land, i.e., the modified IGBP 20-category vegetation types and the STATSGO/FAO 16-category soil texture classes, are also used in GLDAS-2.0. The GLDAS-2.0 data are archived and distributed on the Goddard Earth Sciences Data and Information Services Center website (https://hydro1.gesdisc.eosdis.nasa.gov/data/GLDAS).

The NCEP CFSR is a weakly coupled land–atmosphere–ocean–sea ice global reanalysis system, which uses the NASA Land Information System (LIS) and Noah-LSM model to perform its land surface analysis (Meng et al., 2012). It covers the period from 1979 with a 6-hourly assimilation cycle, and the spatial resolution is T382 Gaussian before 2010 and T574 Gaussian since 2011. In the CFSR/LIS, most of the forcing variables are from the CFSR global atmospheric data assimilation system (GDAS) except for precipitation. Global observed precipitation is introduced to drive the Noah model, as is done in the CRA-Interim/Land. At 0000 UTC each day, the simulated soil temperature and moisture as well as snow variables of the CFSR/LIS are inserted into the CFSR restart file as the land surface initial conditions for the next assimilation cycle.

### 2.2 *The LSM in CRA-Interim/Land*

The LSM used in CRA-Interim/Land is the Noah LSM, which was developed with substantial upgrades from the OSU (Oregon State University) LSM and continued to benefit from a steady progression of improvements (Chen et al., 1997; Koren et al., 1999; Ek et al., 2003) as a collaborative effort between NCEP and many other partners from the land–hydrology community. The Noah model serves as the land component in the evolving Weather Research and Forecasting (WRF) regional atmospheric model, the NOAA NCEP coupled Climate Forecast System (CFS), and the Global Forecast System (GFS). The model simulates the soil freeze–thaw process and its impact on soil heating/cooling and transpiration, following the approach proposed by Koren et al. (1999). It has 4 soil layers with spatially invariant thicknesses of 10, 30, 60, and 100 cm. The first three layers form the root zone in non-forested regions, with the fourth layer included in forested regions.

Every land model is characterized by a specific equilibrium land surface climatology, and the spin-up time required to drive a land model to its equilibrium is much longer than that for the troposphere. To obtain a reasonable initial state for the Noah model, we use the 10-yr meteorological forcing data described in Section 2.1.1 to drive a 30-yr spin-up run and the values of the last time are taken as the initial conditions on 1 January 2007. Then, a continuous 10-yr simulation from 1 January 2007 to 31 December 2016 is conducted with Noah LSM.

To facilitate the understanding of similarities and differences among the CRA-Interim/Land, GLDAS, and CFSR datasets, we list the main features (spatial domains, resolutions, data periods, meteorological forcings, land surface models, and surface parameters) of the three products in Tables 1, 2. As can be seen, most of the meteorological forcings (SW, LW, $T_{2m}$, $q_{2m}$, $p_s$, $U_{10m}$, and $V_{10m}$), except for precipitation, in the CRA-Interim/Land, GLDAS, and CFSR datasets are generated from the atmospheric reanalysis outputs. For the precipitation, similar blended data, in which the gauge-based observations, satellite-retrievals, and reanalysis outputs are merged together, are used in the CRA-Interim/Land and CFSR, while the bias-corrected reanalysis precipitation is used in the GLDAS. In terms of the surface parameters, the CRA-Interim/Land and GLDAS adopt the same soil/vegetation type data, which include finer classifications than those used in the CFSR. In addition, the three products use the same Noah-LSM, while the Noah model in the CRA-Interim/Land is a newer version.

## 3. Results and discussion

To demonstrate the quality of the CRA-Interim/Land

**Table 1.** Summary of the spatial domain, resolution, and data periods of the CRA-Interim/Land, GLDAS, and CFSR products

| Product name | Domain, resolution | Data period |
|---|---|---|
| CRA-Interim/Land | Global, ~34 km, 6-hourly | 2007–2016 (will be extended to 1979–2018 and 3-hourly resolution by the end of 2019) |
| GLDAS | North of 60°S, 0.25°, 3-hourly | 1948–2010 |
| CFSR | Global, ~38 km (1979–2010) and ~27 km (2011–present), 6-hourly | 1979–present |

**Table 2.** Summary of the forcing, LSM, and soil/vegetation parameters of the CRA-Interim/Land, GLDAS, and CFSR products (SW: downward shortwave radiation; LW: downward longwave radiation; $P$: precipitation; $p_s$: surface pressure; $T_{2m}$: 2-m air temperature; $q_{2m}$: 2-m specific humidity; $U_{10m}$: 10-m zonal wind speed; $V_{10m}$: 10-m meridional wind speed)

| Product name | Meteorological forcing | LSM | Soil/vegetation parameter |
|---|---|---|---|
| CRA-Interim/Land | CRA-Interim reanalysis (SW, LW, $T_{2m}$, $q_{2m}$, $p_s$, $U_{10m}$, $V_{10m}$), blended $P$ by using gauge-based observations, satellite-retrievals, and CRA-Interim $P$ | Noah 3.3 | MODIS-based 20-category vegetation and STATSGO/FAO 16-class soil type data |
| GLDAS | Bias-corrected reanalysis ($P$, SW, LW, $T_{2m}$, $q_{2m}$, $p_s$, $U_{10m}$, $V_{10m}$) generated from Princeton University (Sheffield et al., 2006) | Noah 2.7.1 | MODIS-based 20-category vegetation and STATSGO/FAO 16-class soil type data |
| CFSR | NCEP GDAS reanalysis (SW, LW, $T_{2m}$, $q_{2m}$, $p_s$, $U_{10m}$, $V_{10m}$), blended $P$ by using gauge-based observations, satellite-retrievals, and GDAS $P$ | Noah 2.7.1 | AVHRR-based 13-category vegetation and Zobler 9-class soil type data |

product, we compare it with other similar global land products and in situ observations in China.

### 3.1 *Evaluation against other global land surface products*

The global climatology derived from the CRA-Interim/Land was compared with those from the GLDAS-2.0 and CFSR land surface products. Considering that the GLDAS-2.0 ends in 2010, the soil moisture and soil temperature climatologies are determined by using data from 2007 to 2010.

#### 3.1.1 *Soil moisture*

Figures 3a–f show the CRA-Interim/Land, GLDAS, and CFSR global monthly mean volumetric soil moisture for the 0–10-cm soil layer in February and July averaged over 2007–2010, and Figs. 4a–f show the results for the 0–200-cm soil layer. The spatial patterns of all the three products are in good agreement and conform to our current knowledge about the global climatology of dry (Australia, Sahara, and the Middle East) and wet (Southeast Asia, northern South America, and central Africa) areas. Compared with the CRA-Interim/Land and GLDAS, CFSR is wetter in the high latitudes of Eurasia and North America and relatively drier in Sahara, central Africa, and Australia. The CRA-Interim/Land and GLDAS adopt the same land surface parameters, including

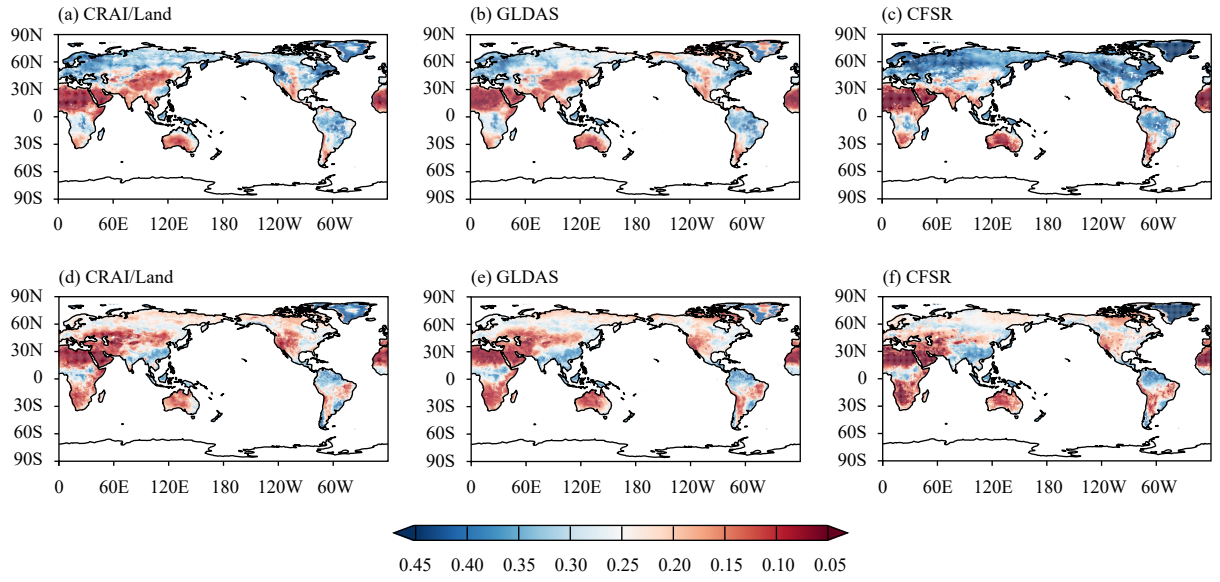


**Fig. 3.** Global monthly mean 0–10-cm volumetric soil moisture ($m^3\ m^{-3}$) climatology (averaged over 2007–2010) derived from (a, d) CRA-Interim/Land, (b, e) GLDAS, and (c, f) CFSR for (a–c) February and (d–f) July.

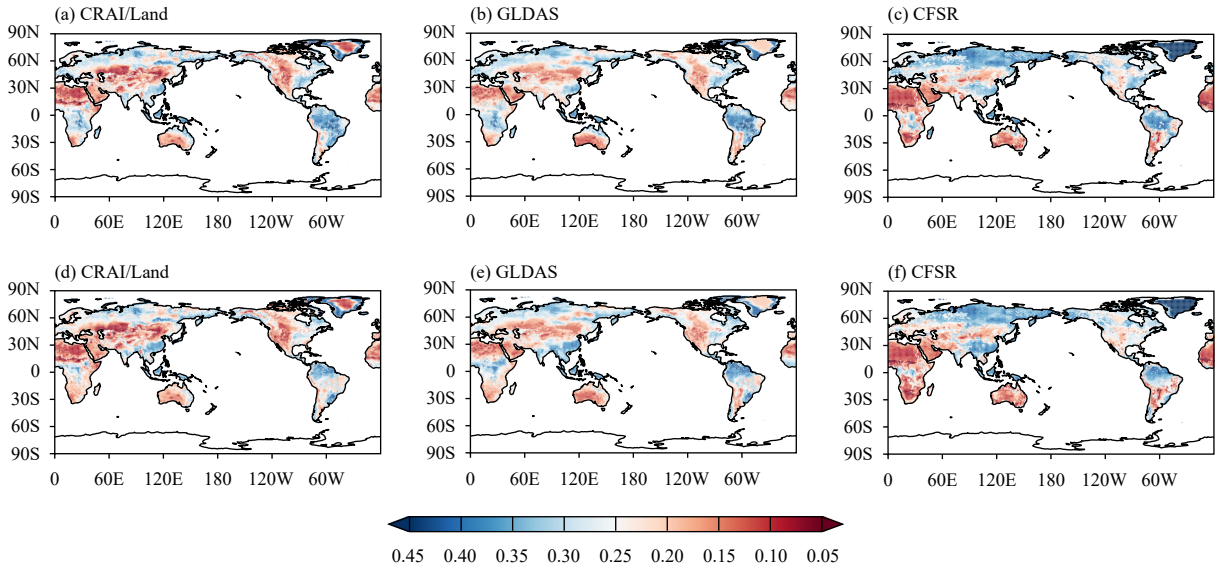


**Fig. 4.** As in Fig. 3, but for 0–200-cm volumetric soil moisture.

the MODIS-based 20-category vegetation and STATSGO/FAO 16-class soil types, while CFSR uses the AVHRR-based 13-category vegetation and Zobler 9-class soil types. We replaced the vegetation and soil-type data in the CRA-Interim/Land with the data used in the CFSR, and compared the soil moisture simulation performance with that of the original CRA-Interim/Land. It was found that the spatial pattern of the resulting soil moisture after changing the vegetation and soil data was much closer to that of the CFSR than the original CRA-Interim/Land (figures omitted). This result implies that differences in the input vegetation and soil-type data may partly account for the spatial pattern differences between the CFSR and the other two datasets.

To assess the skill of the datasets in capturing the seasonal variations, the 0–10-cm soil moisture climatology for 12 months at different latitudes (Figs. 5a–c) and longitudes (Figs. 5d–f) for the CRA-Interim/Land, GLDAS, and CFSR was derived. The three datasets agree well both in the time variations for different latitudes (longit-

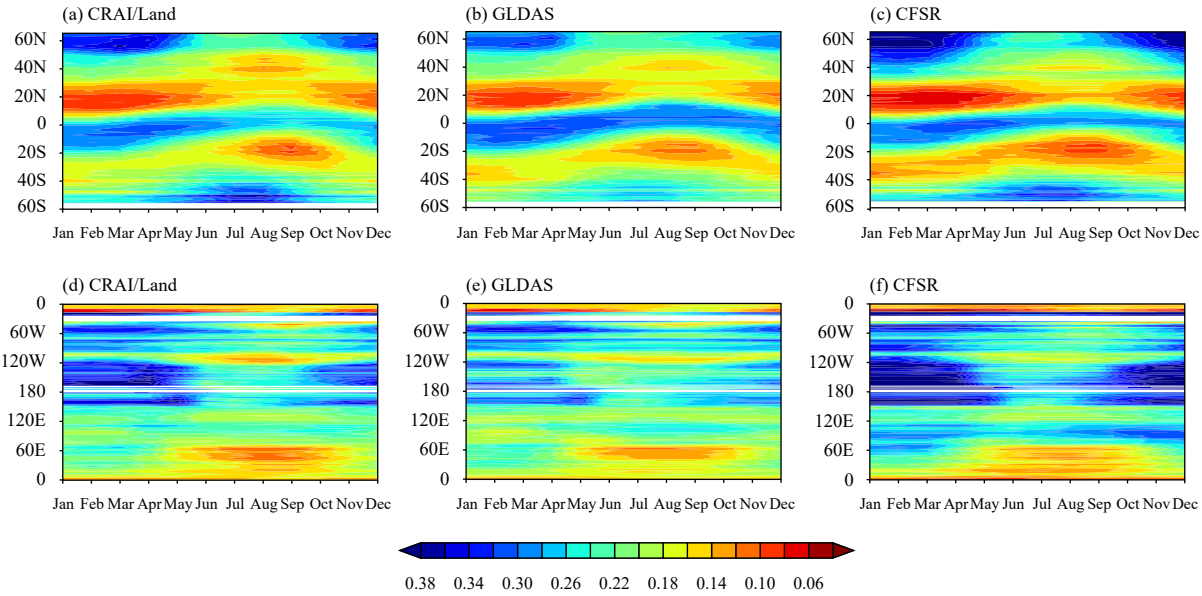


**Fig. 5.** Monthly variations of the (a, d) CRA-Interim/Land, (b, e) GLDAS, and (c, f) CFSR 0–10-cm volumetric soil moisture ($m^3\ m^{-3}$) climatology (averaged over 2007–2010) at different (a–c) latitudes and (d–f) longitudes. The high latitudes north of 65°N and south of 60°S are masked out in (a–c).

udes) and in the spatial variations for different months. It can be seen in Figs. 5a–c that there are notable seasonal variations in the mid- and high-latitude regions, where the soil moisture is wet in winter and spring and dry in summer and autumn. In the tropics, the seasonal fluctuations are weaker than those in the mid and high latitudes, and the soil moisture values of the CRA-Interim/Land lie between the GLDAS (wettest of the three datasets) and CFSR (driest of the three datasets) values. Furthermore, the CRA-Interim/Land and CFSR show notably wet areas for latitudes south of 40°S in winter, while GLDAS shows little information for this area. Figures 5d–f show that for most longitudes, the 0–10-cm soil moisture has evident seasonal variations, with the soil moisture dry from June to September and wet from October to May. Compared with the CRA-Interim/Land and GLDAS, the CFSR soil moisture is wetter in most regions, except for 0°–60°E. Similar to the patterns shown in Fig. 5a–c, at most longitudes, the soil moisture values of the CRA-Interim/Land are in between those of GLDAS and CFSR.

#### 3.1.2 *Soil temperature*

Figures 6a–f depict the CRA-Interim/Land, GLDAS, and CFSR global monthly mean 10-cm soil temperature in February and July averaged over 2007–2010, and Figs. 7a–f show the results for the 40-cm soil temperature. The global patterns of the three products agree well in that temperature peaks in the tropics near the equator and drops along the direction to the mid and high latitudes. In general, CFSR is colder than the CRA-Interim/Land and GLDAS, especially in Sahara, central Africa, the Middle East, and Australia, which are partly due to the different vegetation parameters used in CFSR.

Figures 8a–c show the 10-cm soil temperature climatology for 12 months at different latitudes for the CRA-Interim/Land, GLDAS, and CFSR. It can be seen that the three reanalysis products are in good agreement both in the time variations for different latitudes and in the spatial variations for different months. The seasonal fluctuations of 10-cm soil temperature are obvious in the mid and high latitudes, with high (low) temperature in summer (winter). In the tropics, the seasonal fluctuations are much weaker than those in the mid and high latitudes, with high temperatures throughout most of the year. Compared with the CRA-Interim/Land and GLDAS, the CFSR soil temperature is lower, especially in the tropics and the summer of the Southern Hemisphere. This conforms to the performances when comparing the CFSR with CRA-Interim/Land and GLDAS in Fig. 6.

### 3.2 *Evaluation against ground observations in China*

To evaluate the accuracy of the CRA-Interim/Land, it was compared against in situ observations in China, including the manually measured soil moisture observations at 242 stations (Zhang et al., 2017) and the soil temperature observations at more than 2400 national meteorological automatic stations described in Section 2.1.2.

#### 3.2.1 *Soil moisture*

We checked the spatial performances of the CRA-Interim/Land, GLDAS, and CFSR at the 242 manually measured stations in China using scatterplots of the monthly mean reanalysis versus observed volumetric soil

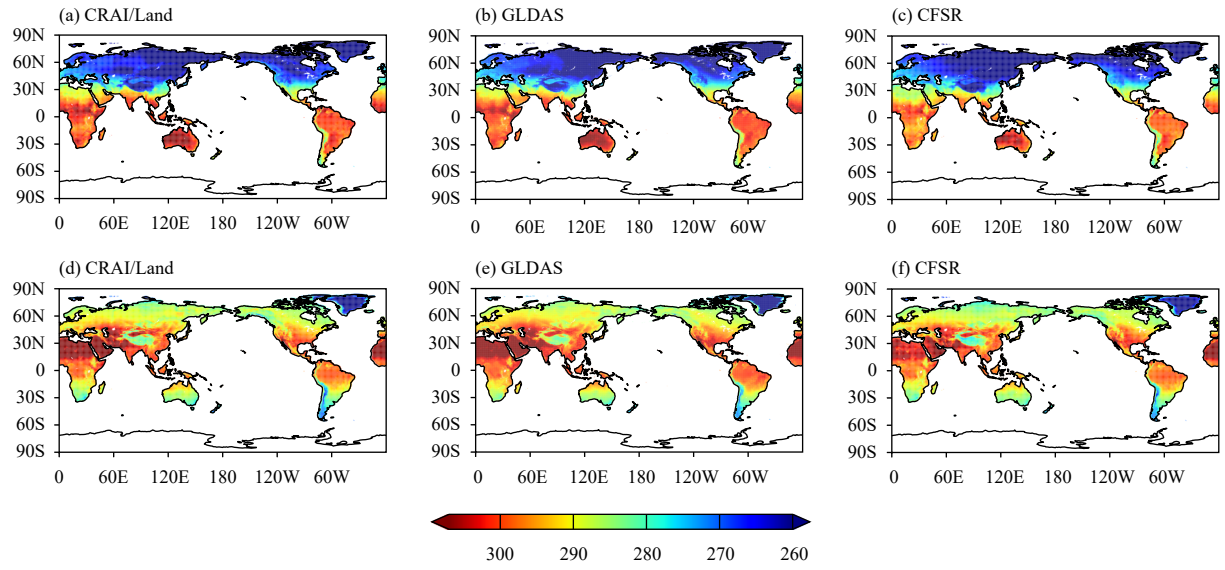


**Fig. 6.** Global monthly mean climatology (averaged over 2007–2010) of soil temperature (K) at 10-cm depth derived from (a, d) CRA-Interim/Land, (b, e) GLDAS, and (c, f) CFSR for (a–c) February and (d–f) July.

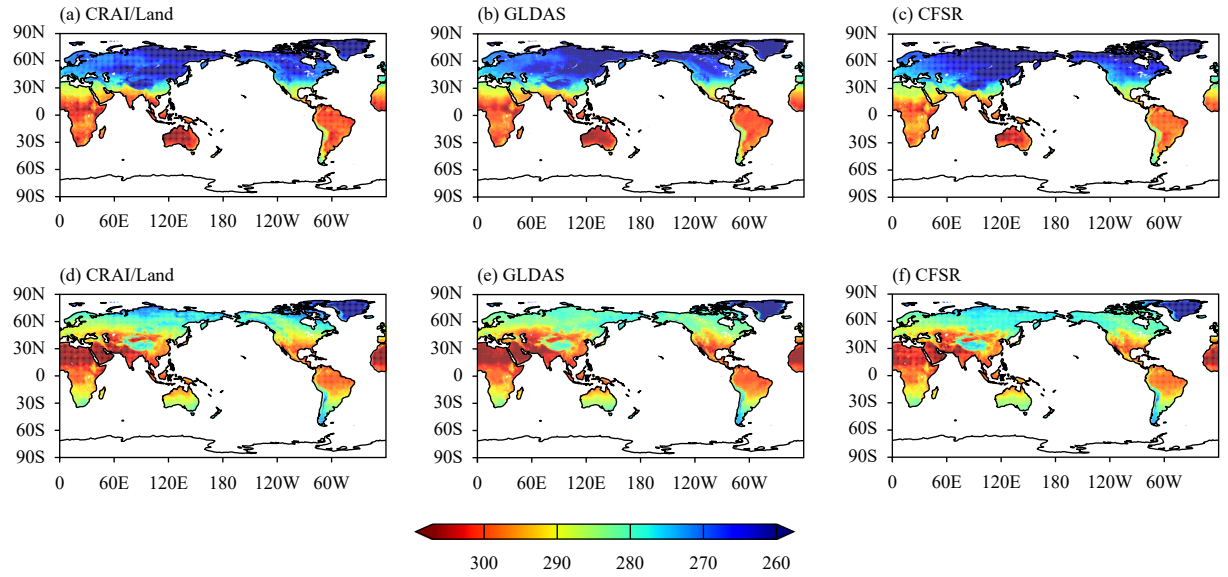


**Fig. 7.** As in Fig. 6, but for soil temperature (K) at 40-cm depth.

moisture ($m^3$ $m^{-3}$) in the 0–10-cm (Figs. 9a–d) and 10–40-cm layers (Figs. 10a–d). In general, all three reanalysis products have positive correlation coefficients with the soil moisture observations. As can be seen from the regression lines and equations, the correlations of the CRA-Interim/Land are the highest among the three datasets in both 0–10 and 10–40 cm layers. To investigate the spatial correlations more clearly, we calculated the spatial correlation of the reanalysis monthly mean soil moisture against monthly mean observations for 2007–2010, as shown in Figs. 11a, b. The CRA-Interim/Land shows higher spatial correlations than the other two products at 0–10 and 10–40 cm, which is in agreement with the results shown in Figs. 9, 10. Furthermore, the spatial correlations in winter and early spring are lower than those in other seasons, which conforms to our current knowledge that land surface models commonly have difficulties in accurately simulating soil moisture in winter and early spring due to the imperfect parameterizations concerning the soil freeze–thaw process.

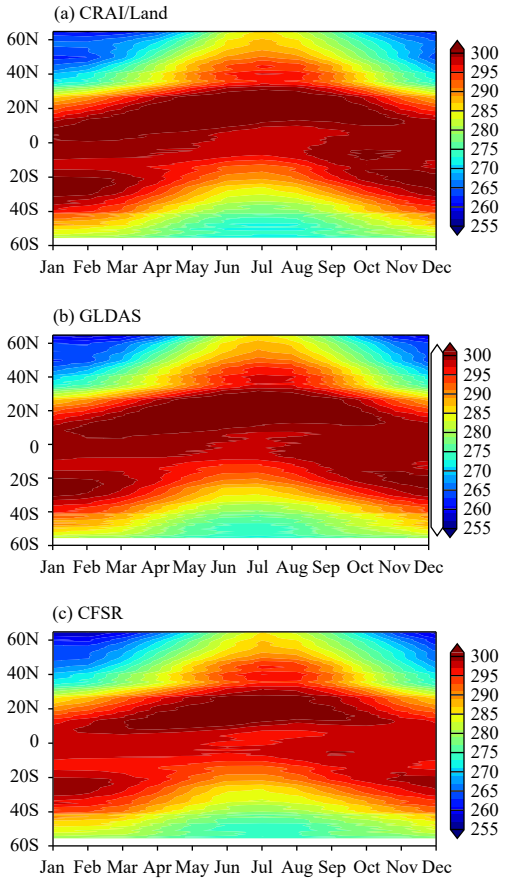


**Fig. 8.** Monthly variations of climatological (averaged over 2007–2010) soil temperature (K) at 10-cm depth from the (a) CRA-Interim/Land, (b) GLDAS, and (c) CFSR at different latitudes. The high latitudes north of 65°N and south of 60°S are masked out.

To assess the temporal performance of three reanalysis datasets in different areas, we derived the temporal bias (Figs. 12a–f), root mean square error (RMSE) (Figs. 13a–f), and correlation coefficient (Figs. 14a–f) of the CRA-Interim/Land, GLDAS, and CFSR monthly mean soil moisture against observations at each station. To facilitate comparison of the three datasets, a histogram showing the value distribution of these metrics is added at the bottom of each figure. In addition, the station-averaged values of these metrics are listed in Table 3. For the 0–10-cm soil layer, the biases (Figs. 12a–c) of the CRA-Interim/Land are in agreement with those of GLDAS, while the CFSR has positive biases in most regions, which are particularly large over Inner Mongolia. From

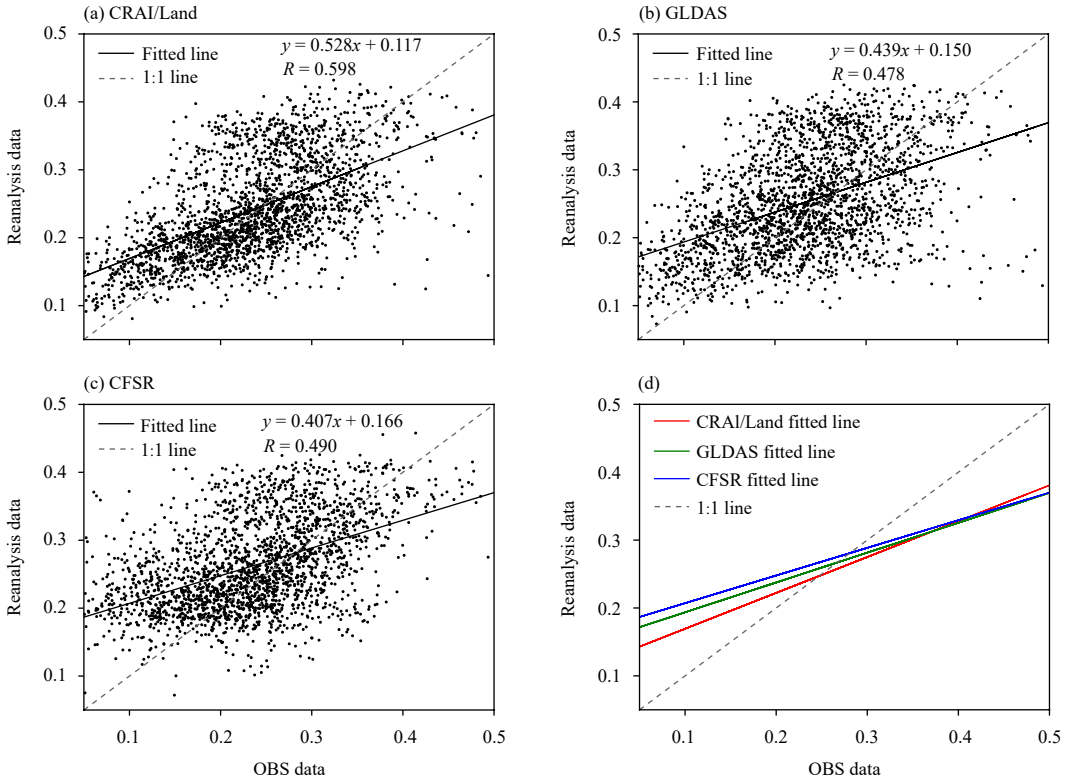


**Fig. 9.** Scatterplots of monthly mean reanalysis and observed 0–10-cm volumetric soil moisture ($m^3\ m^{-3}$) at the manually measured stations in China for (a) CRA-Interim/Land, (b) GLDAS, and (c) CFSR. The regression lines of the three datasets are put together in (d) for comparison.

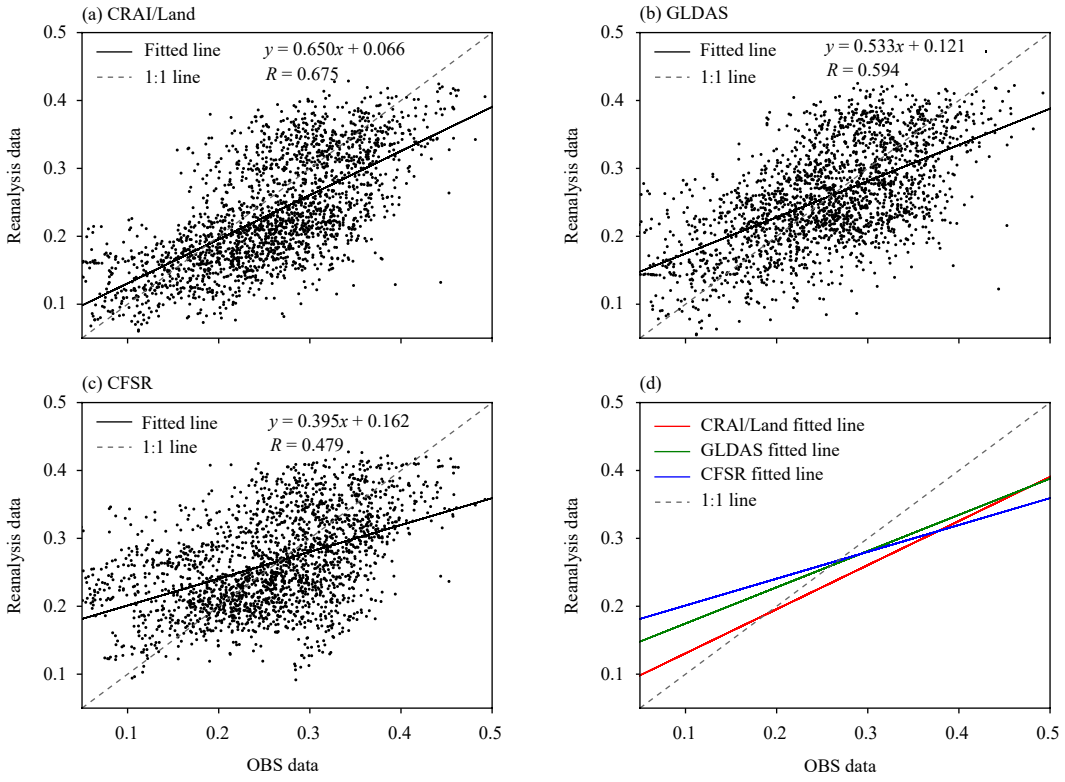


**Fig. 10.** As in Fig. 9, but for the 10–40-cm volumetric soil moisture ($m^3\ m^{-3}$).

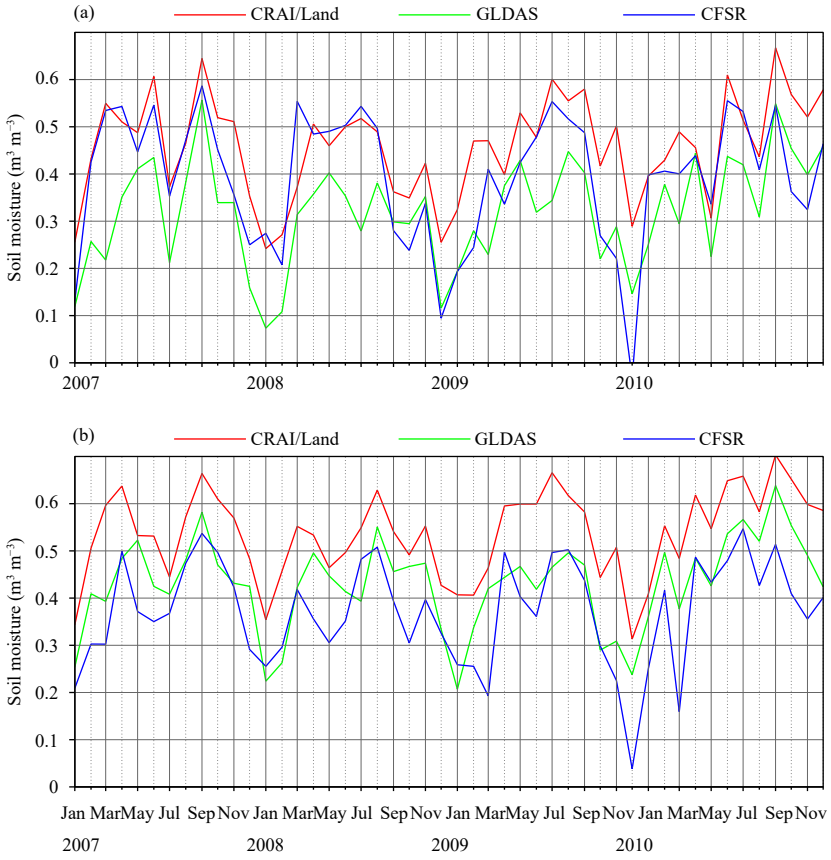


**Fig. 11.** Time series of spatial correlations of the CRA-Interim/Land (red), GLDAS (green), and CFSR (blue) monthly mean soil moisture in the (a) 0–10-cm and (b) 10–40-cm layers during 2007–2010 against the manual measurements at the observation stations in China.

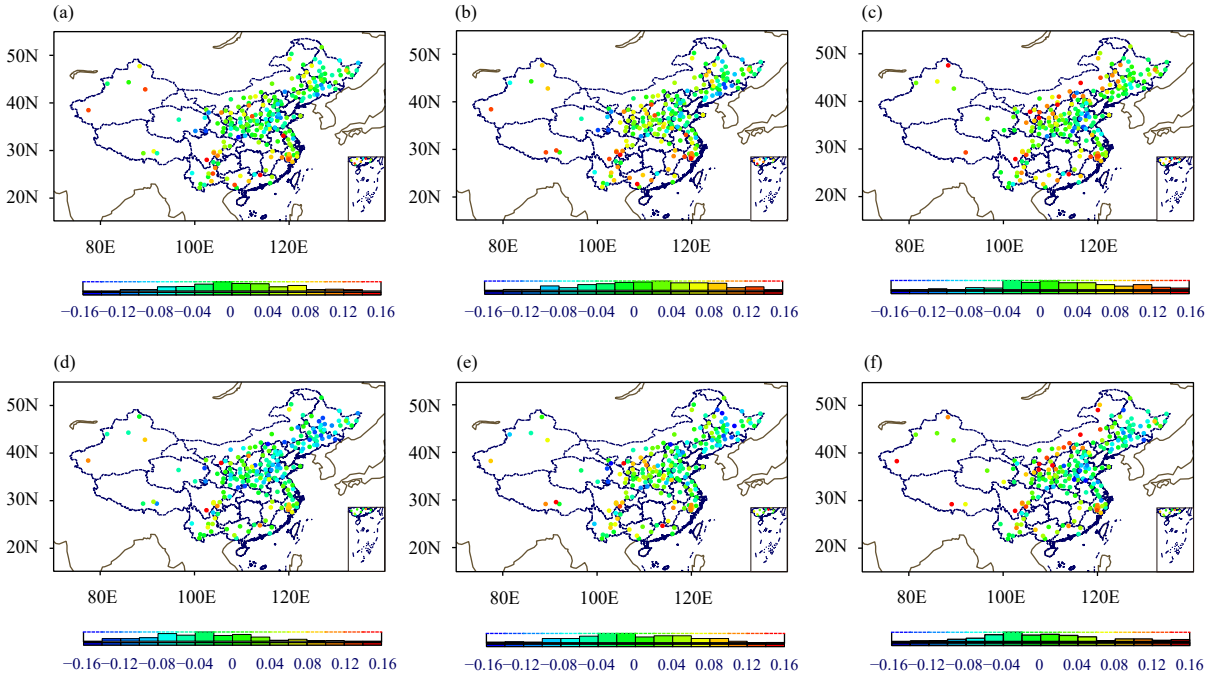


**Fig. 12.** Spatial distributions of temporal bias against observations for the (a, d) CRA-Interim/Land, (b, e) GLDAS, and (c, f) CFSR monthly mean (a–c) 0–10-cm and (d–f) 10–40-cm soil moisture ($m^3$ $m^{-3}$) at the manually measured observation stations in China. The histogram at the bottom of each panel shows the value distribution of the temporal bias.

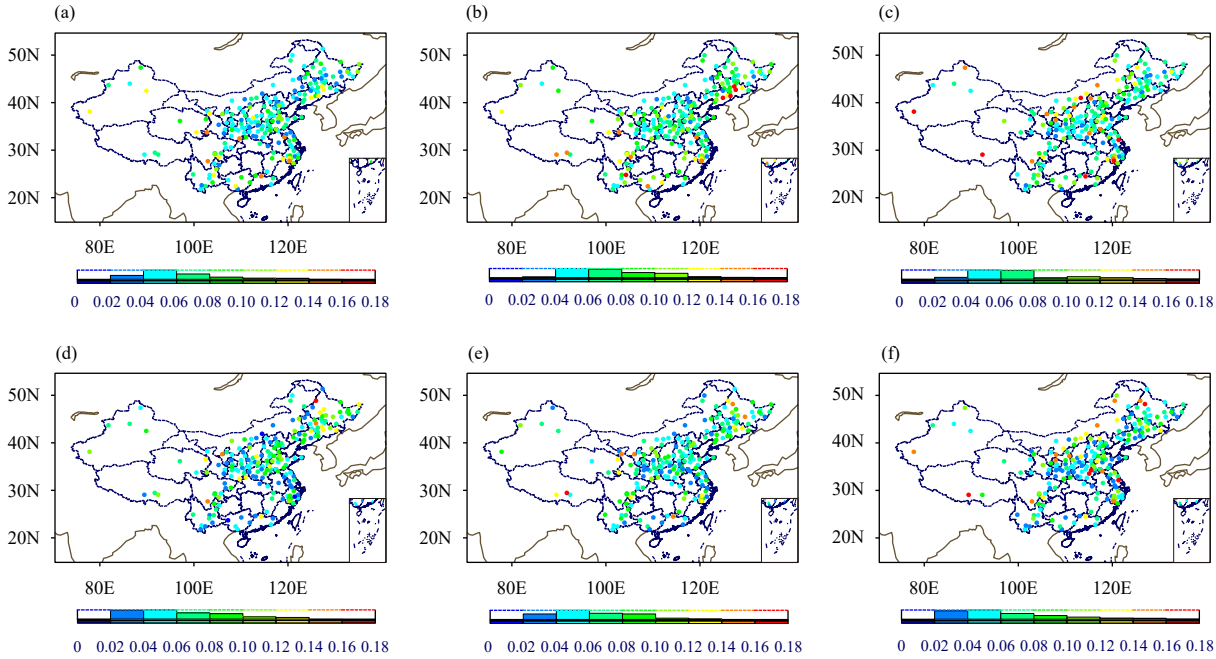


**Fig. 13.** As in Fig. 12, but for the temporal RMSE ($m^3\ m^{-3}$).

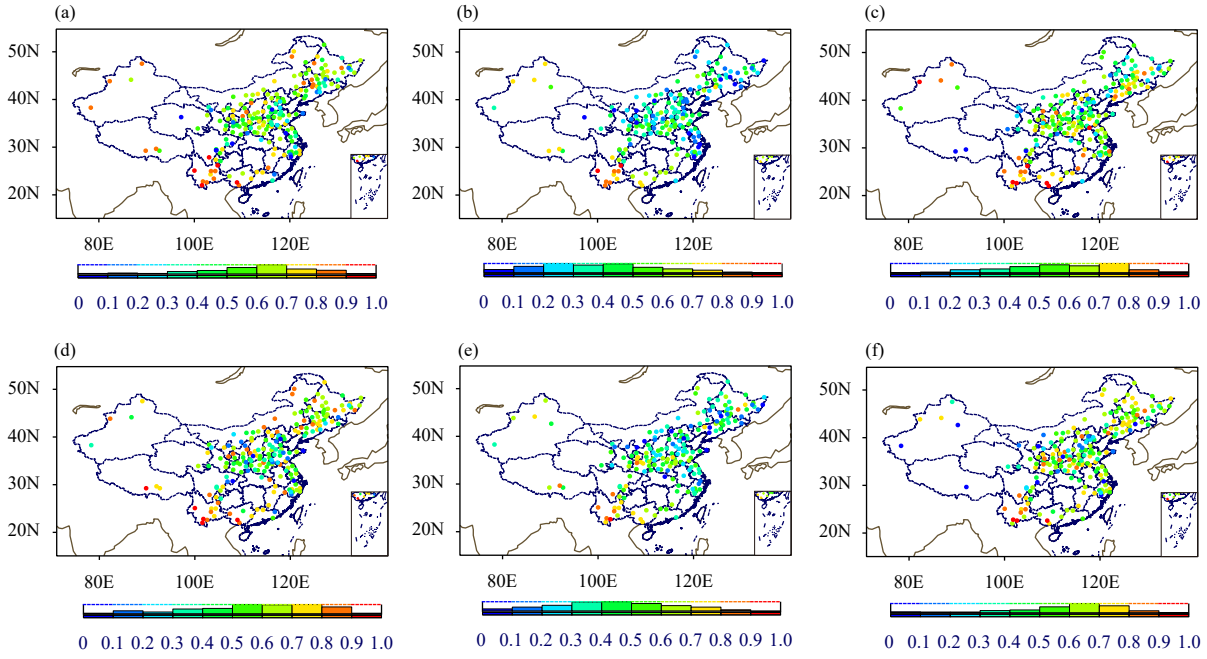


**Fig. 14.** As in Fig. 12, but for the temporal correlation coefficient.

the histograms, we can see more clearly that the bias distributions of the CRA-Interim/Land and GLDAS are close to the normal distribution, while the CFSR obviously has a positively skewed distribution. The station-averaged biases for the CRA-Interim/Land, GLDAS, and CFSR are −0.007, 0.016, and 0.028 $m^3\ m^{-3}$, respectively. For the RMSEs of the 0–10-cm layer (Figs. 13a–c), the CRA-Interim/Land behaves the best among the three datasets especially in northern and central China (30°–50°N, 105°–130°E). The histograms and Table 3 also show that the CRA-Interim/Land has a slightly lower RMSE than the GLDAS and CFSR. For the correlation coefficients of the 0–10-cm layer (Figs. 14a–c), the CRA-Interim/Land performs comparably to the CFSR in most regions, while the GLDAS has relatively lower correlations, especially in central and East China.

**Table 3.** Temporal correlation, bias, and RMSE of the CRA-Interim/Land, GLDAS, and CFSR monthly mean volumetric soil moisture ($m^3\ m^{-3}$) averaged over the agricultural meteorological observation stations in China

| | | Correlation | Bias | RMSE |
|---|---|---|---|---|
| 0–10 cm | CRA-Interim/Land | 0.535 | −0.007 | 0.070 |
| | GLDAS | 0.315 | 0.016 | 0.084 |
| | CFSR | 0.519 | 0.028 | 0.081 |
| 10–40 cm | CRA-Interim/Land | 0.530 | −0.025 | 0.069 |
| | GLDAS | 0.389 | −0.004 | 0.071 |
| | CFSR | 0.514 | 0.007 | 0.074 |

For the 10–40-cm soil layer, the biases of the three products (Figs. 12d–f) behave similarly in Southeast, Southwest, and Northwest China, while the CRA-Interim/land has larger negative biases in Northeast China and north of central China and the CFSR shows larger positive biases over Inner Mongolia. The station-averaged bias values for the CRA-Interim/Land, GLDAS, and CFSR are −0.025, −0.004, and 0.007 $m^3\ m^{-3}$, respectively. The RMSEs of the three datasets (Figs. 13d−f) are roughly at the same level, except that the RMSEs in Inner Mongolia are the lowest for the CRA-Interim/Land and the highest for CFSR. The correlation coefficients (Figs. 14d−f) of the CRA-Interim/Land and CFSR are comparable to each other, with the CRA-Interim/Land better in the regions of Inner Mongolia and Northwest China and the CFSR better in central China. Similar to the results for the 0−10-cm layer, the GLDAS correlations are the lowest in central and East China. Similar analysis results can be seen in the Table 3.

It is shown that the CRA-Interim/Land is drier than the other two datasets and the observations, particularly for the deeper soil layer of 10–40 cm. We found that the screen-level humidity forcing data are underestimated compared with the in situ observations in China. Moreover, further experiments showed that increasing the humidity is useful to partly correct the negative biases in the soil moisture (figures omitted here). Therefore, it can be inferred that the drier biases in the CRA-Interim/Land soil moisture are partly related to the underestimation of the humidity forcing, and assimilating observations into the reanalysis humidity should improve the CRA-Interim/Land soil moisture. In addition, the underestimation of precipitation forcing in China may be another source that leads to the negative biases in the soil moisture, but further analysis is ongoing to investigate this issue.

### 3.2.2 *Ground temperature and soil temperature*

In this section, we compare the performance of the CRA-Interim/Land and CFSR on the basis of observations from more than 2400 automatic stations in China during 2007–2016. Since GLDAS-2.0 ends at 2010, the evaluation results are not determined for GLDAS here. Figures 15a−c show the time series of monthly mean ground temperature, and 10- and 40-cm soil temperature anomalies averaged over the observation stations for the CRA-Interim/Land, CFSR, and observations. The anomaly correlations between the two products and the observations for soil temperature at different depths are listed in Table 4. We can see that the time series of anomalies for both the CRA-Interim/Land and CFSR agree well with those of the observations, and the anomaly correlations of the two products are comparably high.

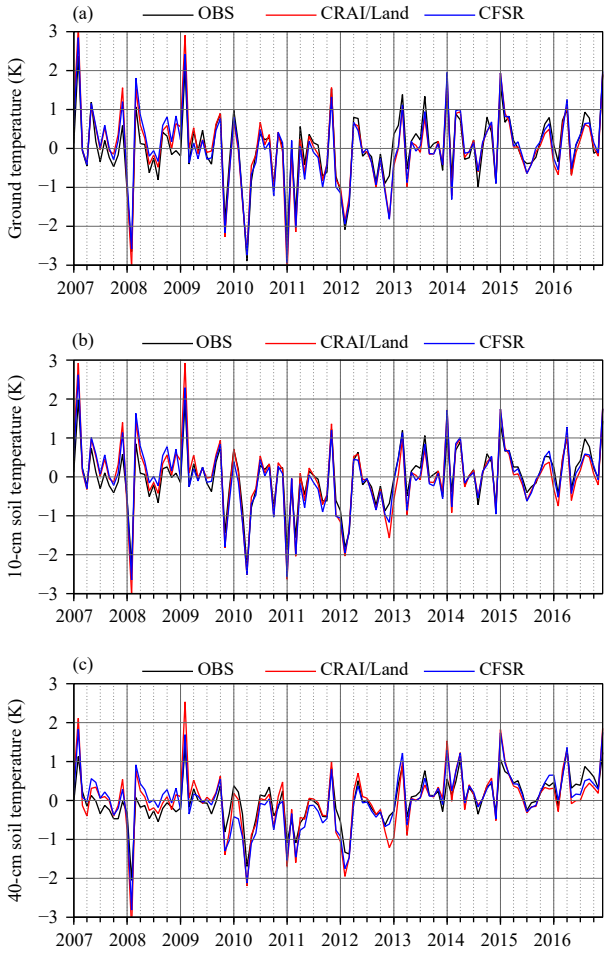


**Fig. 15.** Time series of monthly mean anomalies (K) of (a) ground temperature, and soil temperature (b) at 10-cm depth and (c) at 40-cm depth averaged over the 2400+ national ground meteorological stations in China for observations (black), CRA-Interim/Land (red), and CFSR (blue).

**Table 4.** Temporal anomaly correlations between CRA-Interim/Land, CFSR, and the observations for ground temperature, and 10- and 40-cm soil temperatures

| | Ground | 10 cm | 40 cm |
|---|---|---|---|
| CRA-Interim/Land | 0.95 | 0.96 | 0.91 |
| CFSR | 0.94 | 0.95 | 0.92 |

Figures 16a and 16b show scatterplots of monthly mean reanalysis and observed ground temperature and 10-cm soil temperature (K) at over 2400 national ground meteorological stations in China for the CRA-Interim/Land and CFSR. The results for 40-cm soil temperature are similar to those for 10 cm (figure omitted). In general, the two reanalysis products have comparably high correlation coefficients ($R$ = 0.96−0.97) with the observations, while the bias of the CRA-Interim/Land is lower than that of the CFSR (−3.45 versus −4.02 K for ground temperature and −2.87 versus −3.66 K for 10-cm soil temperature). Moreover, the distribution spread of the CRA-Interim/Land scatter points is smaller than that of the CFSR, indicating that the CRA-Interim/Land has fewer abnormal values. Compared with the observations, both of the datasets underestimate ground and soil temperature at most of the observation stations.

To understand the temporal performances of reanalysis datasets in different regions, we derived the temporal bias (Figs. 17a–d) and RMSE (Figs. 18a–d) of the CRA-Interim/Land and CFSR monthly mean soil temperature against observations at each station. Compared with the in situ observations, both reanalysis products show negative biases, especially for the ground temperature, indicating that the reanalyses underestimate the temperature. This is consistent with previous studies on the evaluation of simulated land surface temperature in China (e.g., Sun et al., 2017; Zhou et al., 2017). The biases and RMSEs of ground temperature and 10-cm soil temperature show a similar pattern of larger error metrics in West and Northeast China, and much smaller ones in central, Southeast, and South China. Compared with the CFSR, the CRA-Interim/Land has notably lower biases and RMSEs mainly in East and central China (20°–40°N, 100°–125°E). The histograms in Figs. 17, 18 depict more clearly that the CRA-Interim/Land has fewer stations with large negative biases (bias < −3 K) and large RMSEs (RMSE > 3.5 K) than the CFSR. We also calculated the station-averaged values of these metrics (Table 5). Similar to the results shown in Figs. 17, 18, the station-averaged biases and RMSEs of the CRA-Interim/Land are smaller than those of the CFSR in different soil layers. The CRA-Interim/Land uses the MODIS IGBP 20-category vegetation data, which have been verified to have a positive effect on the simulation of surface temperature in several studies (e.g., Li et al., 2018). The results for the 40-cm soil temperature are similar to those for 10 cm (figure omitted).

## 4. Summary

In 2014, the CMA has started its mission to producing China's first generation of a 40-yr global atmospheric reanalysis product (CRA-40). Recently, a 10-yr global land surface reanalysis interim dataset named CRA-Interim/Land (2007–2016, approximately 34-km Gaussian grid, 6-h intervals) has been produced and is introduced in this paper. The present work documents its implementation and evaluation results. The CRA-Interim/Land is generated by the Noah-LSM in an offline mode forced by near-surface meteorological fields from the companion CRA-Interim atmospheric reanalysis output, along with observation-based global precipitation analysis to alleviate biases in the reanalysis precipitation. The resulting global soil moisture and the soil temperature in different soil layers are validated by using the GLDAS and CFSR global land surface datasets and in situ observations in China.

It is shown that the global spatial patterns and monthly variations of the CRA-Interim/Land, GLDAS, and CFSR climatology are highly consistent, and the soil moisture and temperature values of the CRA-Interim/Land dataset

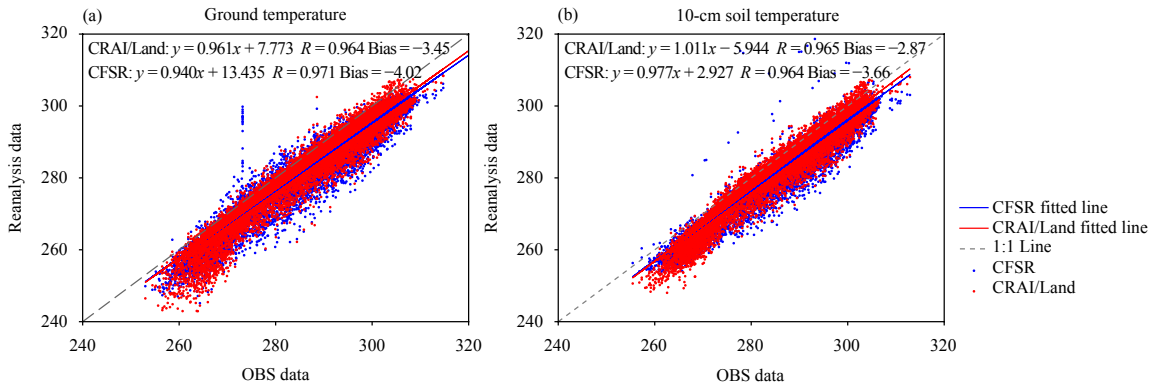


**Fig. 16.** Scatterplots of monthly mean reanalysis and observed (a) ground temperature and (b) 10-cm soil temperature (K) at 2400+ national ground meteorological stations in China for CRA-Interim/Land (red) and CFSR (blue).

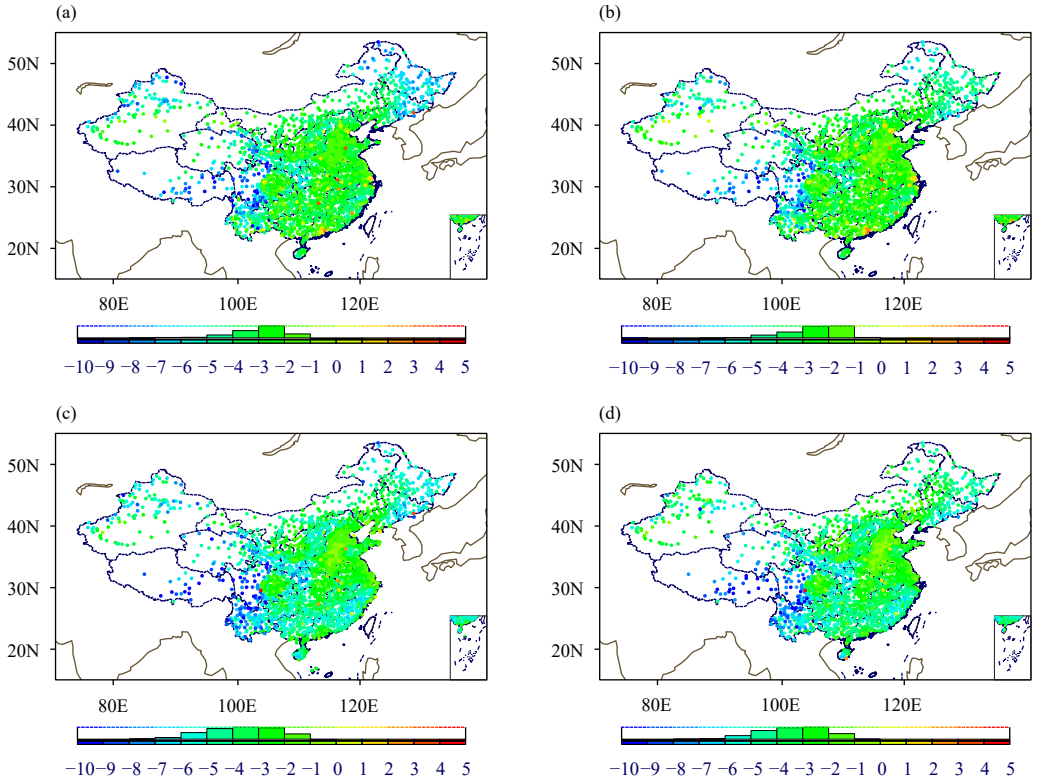


**Fig. 17.** Spatial distributions of temporal bias against observations for the (a, b) CRA-Interim/Land and (c, d) CFSR monthly mean (a, c) ground temperature and (b, d) 10-cm soil temperature (K) at 2400+ national ground meteorological stations in China. The histogram at the bottom of each panel shows the value distribution of the temporal bias. The results for 40-cm soil temperature are similar and not shown.

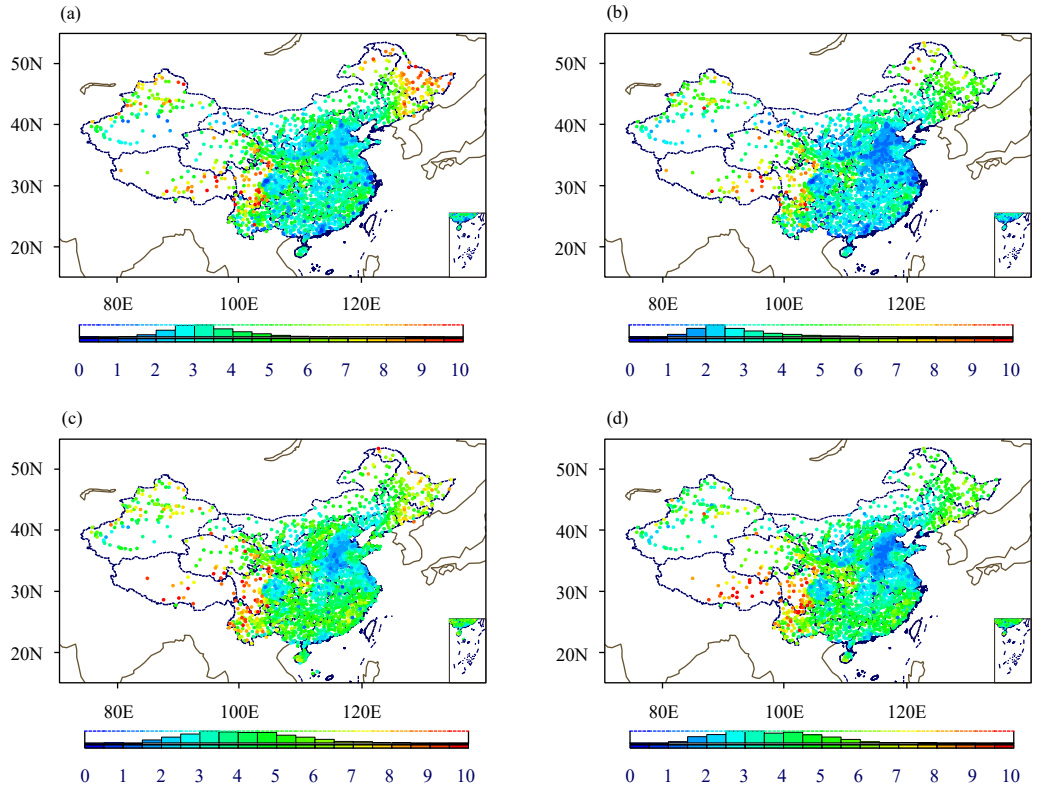


**Fig. 18.** As in Fig. 17, but for the temporal RMSE (K).

**Table 5.** Temporal bias and RMSE of the CRA-Interim/Land and CFSR monthly mean soil temperature (K) averaged over the national ground meteorological stations in China

| | | Bias (K) | RMSE (K) |
|---|---|---|---|
| Ground temperature | CRA-Interim/Land | –3.45 | 3.98 |
| | CFSR | –3.88 | 4.65 |
| 10-cm soil temperature | CRA-Interim/Land | –2.87 | 3.29 |
| | CFSR | –3.63 | 4.16 |

lie in between those of the GLDAS and CFSR datasets. Evaluated against ground observations in China, the CRA-Interim/Land soil moisture is comparable to or better than those of the GLDAS and CFSR for the 0–10-cm soil layer and has higher correlations and slightly lower RMSEs for the 10–40-cm soil layer. However, it shows evident negative biases for the 10–40-cm soil moisture in Northeast China and north of central China. Current experiments show that such negative biases may partly result from the underestimation of screen-level humidity and precipitation forcing, but further analysis is ongoing to investigate this issue. For the ground temperature and soil temperature in different layers, the CRA-Interim/Land performs better than the CFSR in that the CRA-Interim/Land has lower biases and RMSEs and comparably high correlations compared with the CFSR.

The CRA-Interim/Land has added value over the land components of the CRA-Interim reanalysis with the incorporation of global precipitation observations and improved soil/vegetation parameters, and therefore can potentially better serve the needs of studies on land-surface hydrology, climate, and weather. Further work on more in-depth evaluation and investigation of the CRA-Interim/Land, assimilation of near-surface atmospheric forcing variables, as well as extension of the current dataset to 40 yr (1979–2018; CRA-40/Land) is ongoing.

## REFERENCES


Balsamo, G., C. Albergel, A. Beljaars, et al., 2015: ERA-Interim/Land: A global land surface reanalysis data set. *Hydrol. Earth Syst. Sci.*, **19**, 389–407, doi: 10.5194/hess-19-389-2015.

Chen, F., Z. Janjić, and K. Mitchell, 1997: Impact of atmospheric surface-layer parameterizations in the new land-surface scheme of the NCEP Mesoscale Eta model. *Bound.-Layer Meteor.*, **185**, 391–421, doi: 10.1023/A:1000531001463.

Chen, Y. Y., K. Yang, J. Qin, et al., 2013: Evaluation of AMSR-E retrievals and GLDAS simulations against observations of a soil moisture network on the central Tibetan Plateau. *J. Geophys. Res. Atmos.*, **118**, 4466–4475, doi: 10.1002/jgrd.50301.

Decharme, B., and H. Douville, 2006: Uncertainties in the GSWP-2 precipitation forcing and their impacts on regional and global hydrological simulations. *Climate Dyn.*, **27**, 695–713, doi: 10.1007/s00382-006-0160-6.

Decker, M., M. A. Brunke, Z. Wang, et al., 2012: Evaluation of the reanalysis products from GSFC, NCEP, and ECMWF using flux tower observations. *J. Climate*, **25**, 1916–1944, doi: 10.1175/JCLI-D-11-00004.1.

Dorigo, W., R. de Jeu, D. Chung, et al., 2012: Evaluating global trends (1988–2010) in harmonized multi-satellite surface soil moisture. *Geophys. Res. Lett.*, **39**, L18405, doi: 10.1029/2012GL052988.

Ek, M. B., K. E. Mitchell, Y. Lin, et al., 2003: Implementation of Noah land surface model advances in the National Centers for Environmental Prediction operational mesoscale Eta model. *J. Geophys. Res. Atmos.*, **108**, 8851, doi: 10.1029/2002JD003296.

Fekete, B. M., C. J. Vörösmarty, J. O. Roads, et al., 2004: Uncertainties in precipitation and their impacts on runoff estimates. *J. Climate*, **17**, 294–304, doi: 10.1175/1520-0442(2004)017<0294:UIPATI>2.0.CO;2.

Friedl, M. A., D. Sulla-Menashe, B. Tan, et al., 2010: MODIS Collection 5 global land cover: Algorithm refinements and characterization of new datasets. *Remote Sens. Environ.*, **114**, 168–182, doi: 10.1016/j.rse.2009.08.016.

Gao, Y. H., L. Cuo, and Y. X. Zhang, 2014: Changes in moisture flux over the Tibetan Plateau during 1979–2011 and possible mechanisms. *J. Climate*, **27**, 1876–1893, doi: 10.1175/JCLI-D-13-00321.1.

Gottschalck, J., J. Meng, M. Rodell, et al., 2005: Analysis of multiple precipitation products and preliminary assessment of their impact on Global Land Data Assimilation System land surface states. *J. Hydrometeor.*, **6**, 573–598, doi: 10.1175/JHM437.1.

Guo, Z. C., P. A. Dirmeyer, Z.-Z. Hu, et al., 2006: Evaluation of the Second Global Soil Wetness Project soil moisture simulations: 2. Sensitivity to external meteorological forcing. *J. Geophys. Res. Atmos.*, **111**, D22S03, doi: 10.1029/2006JD007845.

Henry, C. M., D. M. Allen, and J. L. Huang, 2011: Groundwater storage variability and annual recharge using well-hydrograph and GRACE satellite data. *Hydrogeol. J.*, **19**, 741–755, doi: 10.1007/s10040-011-0724-3.

Janowiak, J. E., A. Gruber, C. R. Kondragunta, et al., 1998: A comparison of the NCEP–NCAR reanalysis precipitation and the GPCP rain gauge–satellite combined dataset with observational error considerations. *J. Climate*, **11**, 2960–2979, doi: 10.1175/1520-0442(1998)011<2960:ACOTNN>2.0.CO;2.

Ji, L., G. B. Senay, and J. P. Verdin, 2015: Evaluation of the Global Land Data Assimilation System (GLDAS) air temperature data products. *J. Hydrometeor.*, **16**, 2463–2480, doi: 10.1175/JHM-D-14-0230.1.

Jiménez, C., C. Prigent, B. Mueller, et al., 2011: Global intercomparison of 12 land surface heat flux estimates. *J. Geophys. Res. Atmos.*, **116**, D02102, doi: 10.1029/2010JD014545.

Joaquin, M.-S., E. Dutra, G. Balsamo, et al., 2017: ERA5-Land: A new state-of-the-art global land surface reanalysis dataset. Proc. 31st Conference on Hydrology, 25 January, Amer. Meteor. Soc., Seattle, US, 1–16.

Kim, S., R. M. Parinussa, Y. Y. Liu, et al., 2015: A framework for combining multiple soil moisture retrievals based on maximizing temporal correlation. *Geophys. Res. Lett.*, **42**, 6662–6670, doi: 10.1002/2015GL064981.

Koren, V., J. Schaake, K. Mitchell, et al., 1999: A parameterization of snowpack and frozen ground intended for NCEP weather and climate models. *J. Geophys. Res. Atmos.*, **104**,

19,569–19,585, doi: 10.1029/1999JD900232.

Li, Y. H., C. L. Zhao, T. J. Zhang, et al., 2018: Impacts of land-use data on the simulation of surface air temperature in Northwest China. *J. Meteor. Res.*, **32**, 896–908, doi: 10.1007/s13351-018-7151-5.

Liu, D., G. L. Wang, R. Mei, et al., 2014: Diagnosing the strength of land–atmosphere coupling at subseasonal to seasonal time scales in Asia. *J. Hydrometeor.*, **15**, 320–339, doi: 10.1175/JHM-D-13-0104.1.

Liu, Y. Y., W. A. Dorigo, R. M. Parinussa, et al., 2012: Trend-preserving blending of passive and active microwave soil moisture retrievals. *Remote Sens. Environ.*, **123**, 280–297, doi: 10.1016/j.rse.2012.03.014.

Liu, Z. Q., C. X. Shi, Z. J. Zhou, et al., 2017: CMA global reanalysis (CRA-40): Status and plans. Proc. 5th International Conference on Reanalysis, 13–17 November, Natl. Meteor. Int. Center, Rome, Italy, 1–16.

Long, D., B. R. Scanlon, L. Longuevergne, et al., 2013: GRACE satellite monitoring of large depletion in water storage in response to the 2011 drought in Texas. *Geophys. Res. Lett.*, **40**, 3395–3401, doi: 10.1002/grl.50655.

Materia, S., P. A. Dirmeyer, Z. C. Guo, et al., 2010: The sensitivity of simulated river discharge to land surface representation and meteorological forcings. *J. Hydrometeor.*, **11**, 334–351, doi: 10.1175/2009JHM1162.1.

Maurer, E. P., G. M. O'Donnell, D. P. Lettenmaier, et al., 2001: Evaluation of the land surface water budget in NCEP/NCAR and NCEP/DOE reanalyses using an off-line hydrologic model. *J. Geophys. Res. Atmos.*, **106**, 17841–17862, doi: 10.1029/2000JD900828.

Meng, J., R. Q. Yang, H. L. Wei, et al., 2012: The land surface analysis in the NCEP Climate Forecast System Reanalysis. *J. Hydrometeor.*, **13**, 1621–1630, doi: 10.1175/JHM-D-11-090.1.

Proulx, R. A., M. D. Knudson, A. Kirilenko, et al., 2013: Significance of surface water in the terrestrial water budget: A case study in the Prairie Coteau using GRACE, GLDAS, Landsat, and groundwater well data. *Water Resour. Res.*, **49**, 5756–5764, doi: 10.1002/wrcr.20455.

Reichle, R. H., R. D. Koster, G. J. M. De Lannoy, et al., 2011: Assessment and enhancement of MERRA land surface hydrology estimates. *J. Climate*, **24**, 6322–6338, doi: 10.1175/JCLI-D-10-05033.1.

Ren, Z. H., Z. F. Zhang, C. Sun, et al., 2015: Development of three-step quality control system of real-time observation data from AWS in China. *Meteor. Mon.*, **41**, 1268–1277, doi: 10.7519/j.issn.1000-0526.2015.10.010. (in Chinese)

Rodell, M., P. R. Houser, U. Jambor, et al., 2004: The global land data assimilation system. *Bull. Amer. Meteor. Soc.*, **85**, 381–394, doi: 10.1175/BAMS-85-3-381.

Rodell, M., J. L. Chen, H. Kato, et al., 2007: Estimating groundwater storage changes in the Mississippi River basin (USA) using GRACE. *Hydrogeol. J.*, **15**, 159–166, doi: 10.1007/s10040-006-0103-7.

Sheffield, J., G. Goteti, and E. F. Wood, 2006: Development of a 50-year high-resolution global dataset of meteorological forcings for land surface modeling. *J. Climate*, **19**, 3088–3111, doi: 10.1175/JCLI3790.1.

Sun, S., C. X. Shi, X. Liang, et al., 2017: Assessment of ground temperature simulation in China by different land surface models based on station observations. *J. Appl. Meteor. Sci.*, **28**, 737–749, doi: 10.11898/1001-7313.20170609. (in Chinese)

Wang, A. H., and X. B. Zeng, 2012: Evaluation of multireanalysis products with in situ observations over the Tibetan Plateau. *J. Geophys. Res. Atmos.*, **117**, D05102, doi: 10.1029/2011JD016553.

Xia, Y. L., Z. C. Hao, C. X. Shi, et al., 2019: Regional and global land data assimilation systems: Innovations, challenges, and prospects. *J. Meteor. Res.*, **33**, 159–189, doi: 10.1007/s13351-019-8172-4.

Xie, P. P., and P. A. Arkin, 1997: Global precipitation: A 17-year monthly analysis based on gauge observations, satellite estimates, and numerical model outputs. *Bull. Amer. Meteor. Soc.*, **78**, 2539–2558, doi: 10.1175/1520-0477(1997)078<2539:GPAYMA>2.0.CO;2.

Xie, P. P., A. Yatagai, M. Chen, et al., 2007: A gauge-based analysis of daily precipitation over East Asia. *J. Hydrometeor.*, **8**, 607–626, doi: 10.1175/JHM583.1.

Xue, B.-L., L. Wang, X. P. Li, et al., 2013: Evaluation of evapotranspiration estimates for two river basins on the Tibetan Plateau by a water balance method. *J. Hydrol.*, **492**, 290–297, doi: 10.1016/j.jhydrol.2013.04.005.

Zaitchik, B. F., M. Rodell, and F. Olivera, 2010: Evaluation of the Global Land Data Assimilation System using global river discharge data and a source-to-sink routing scheme. *Water Resour. Res.*, **46**, W06507, doi: 10.1029/2009WR007811.

Zhang, J. Y., W.-C. Wang, and J. F. Wei, 2008: Assessing land–atmosphere coupling using soil moisture from the Global Land Data Assimilation System and observational precipitation. *J. Geophys. Res. Atmos.*, **113**, D17119, doi: 10.1029/2008JD009807.

Zhang, L., H. Q. Lyu, and L. Y. Wang, 2017: Analysis and calibration of singular historical observed data of manual soil water. *Meteor. Mon.*, **43**, 189–196, doi: 10.7519/j.issn.1000-0526.2017.02.006. (in Chinese)

Zhao, B., B. Zhang, C. X. Shi, et al., 2019: Comparison of the global energy cycle between Chinese Reanalysis Interim and ECMWF Reanalysis. *J. Meteor. Res.*, **33**, 563–575, doi: 10.1007/s13351-019-8129-7.

Zhou, C. L., K. C. Wang, and Q. Ma, 2017: Evaluation of eight current reanalyses in simulating land surface temperature from 1979 to 2003 in China. *J. Climate*, **30**, 7379–7398, doi: 10.1175/JCLI-D-16-0903.1.

Tech & Copy Editor: Zhirong CHEN